Atomic Force Microscopy, Electron Paramagnetic Resonance and X-ray Fluorescence Investigations of Self-Assembled Lines from Colloidal Solutions of Lamellar MnO_x

Manuel Marquez,[†] Josh Robinson,[‡] Vincent Van Nostrand,[§] David Schaefer,[‡] Lev R. Ryzhkov,*[,§] Walter Lowe,[‡] and Steven L. Suib[||]

U-60, Department of Chemistry, University of Connecticut, Storrs, Connecticut 06269-3060, Department of Chemistry, Towson University, Towson, Maryland 21252-0001, Department of Physics, Astronomy, and Geosciences, Towson University, Towson, Maryland 21252-0001, MHATT-CAT, Department of Physics, Howard University, 2400 Sixth Street, NW, Washington, D.C. 20059, Los Alamos National Laboratory, Chemical Science and Technology Division, Los Alamos, New Mexico 87545, and Nanotechnology Laboratory, Research and Development, Kraft Foods, Inc., 801 Waukegan Rd, Glenview, Illinois 60025

Received March 30, 2001. Revised Manuscript Received December 21, 2001

In this article, we report AFM, EPR, and X-ray fluorescence studies of well-ordered linear patterns of manganese oxide deposited onto glass and quartz surfaces. The patterns reported here were generated from newly described colloidal solutions of manganese oxide nanoparticles of composition $[N(CH_3)_4]^+_{0.93}Mn^{4+}_{2.1}Mn^{3+}_{1.9}O_7(OH)_{1.03}\cdot 5H_2O$. Qualitative studies, and quantitative analysis of the concentration dependence of the width, frequency, and height of the ordered lines of MnO_x (average Mn oxidation state of 3.52) were performed. These results provide information about the morphology of the patterns, the distribution of Mn within the lines, and the nature of free-radicals detected in this material.

Introduction

There has been recent interest in the synthesis of nanoparticles for preparation of thin films, sensor devices, and novel porous catalysts and adsorbents.[1] Nano- or micrometer scale regular patterns of inorganic films with specific physical properties such as porosity or conductivity[1−9] have led to numerous experimental and theoretical studies. For example, the design of conducting wires via molecular engineering has recently been the focus of several laboratories for potential application as sensors,[1] to enhance computer speed and for energy storage materials,[2] and as effective materials for separation.[3] A multitude of inorganic materials have been utilized for such potential applications.

Substantial progress has been made in controlling the porous structure of inorganic systems.[4] Materials with nano-, meso-, and macropores have been prepared by using structure-directing agents such as small organic molecules, polymers, surfactants, emulsions, and nano- and microspheres.[5−10] Applications of porous materials include separations, catalysis, sensors, molecular recognition, optics, and electronics.[11−13] Control over the orientation and morphology is also important in designing advanced materials. Orientation of inorganic crystals has been achieved by controlled nucleation on glass[14] and polymer surfaces[15] as well as self-assembled monolayers.[16] Materials with curved morphologies ranging from spherical to spiral shapes have been produced in the nanometer through the millimeter scale.[17−19]

[†] Los Alamos National Laboratory and Kraft Foods, Inc.
[‡] Department of Physics, Astronomy, and Geosciences, Towson University, and Howard University.
[§] Department of Chemistry, Towson University.
[||] University of Connecticut.

(1) (a) Wu, C. G.; Bein, T. *Science* **1994**, *264*, 1757−1759. (b) Giraldo, O.; Marquez, M.; Brock, S. L.; Suib, S. L.; Hillhouse, H.; Tsapatsis, M. *J. Am. Chem. Soc.* **2000**, *122*, 12158−12163.
(2) (a) Trau, M.; Yao, N.; Kim, E.; Xia, Y.; Whitesides, G. M.; Aksay, I. A. *Nature* **1997**, *390*, 674−676. (b) Liao, H.; Wang, Y.; Zhang, S.; Yitai, Q. *Chem. Mater.* **2001**, *13*, 6−8.
(3) (a) den Exter, M. J.; Jansen, J. C.; van de Graaf, J. M.; Kapteijn, F.; Moulijn, J. A.; van Bekkum, H. In *Recent Advances and New Horizons in Zeolite Science and Technology*; Chon, H., Woo, S. I., Park, S. E., Eds.; *Studies in Surface Science and Catalysis*; Elsevier: Amsterdam, 1996; Vol. 102, pp 413−454. (b) Fulmer, P.; Raja, M. M.; Manthiram, A. *Chem. Mater.* **2001**, *13*, 2160−2168.
(4) Ferey, G.; Cheetham, A. K. *Science* **1999**, *283*, 1125−1126.
(5) Tian, Z. R.; Tong, W.; Wang, J. Y.; Duan, N.; Krishnan, V. V.; Suib, S. L. *Science* **1997**, *276*, 926−930.
(6) (a) Yang, P.; Zhao, D.; Margolese, D. I.; Chmelka, B. F.; Stucky, G. D. *Nature* **1998**, *396*, 152−155. (b) Gier, T. E.; Bu, X.; Feng, P.; Stucky, G. D. *Nature* **1998**, *395*, 154−157.
(7) Akporiaye, D. E. *Angew. Chem., Int. Ed. Engl.* **1998**, *37*, 2456−2457.
(8) Li, H.; Laine, A.; O'Keeffe, M.; Yaghi, O. M. *Science* **1999**, *283*, 1145−1147.
(9) (a) Holland, B. T.; Blanford, C. F.; Stein, A. *Science* **1998**, *281*, 538−540. (b) Caruso, F.; Caruso, R. A.; Mohwald, H. *Science* **1998**, *282*, 1111−1114.
(10) Walsh, D.; Hopwood, J. D.; Mann, S. *Science* **1994**, *264*, 1576−1579.
(11) *Handbook of Heterogeneous Catalysis*; Ertl, G., Knozinger, H., Weitkamp, J., Eds.; Wiley-VCH: New York, 1997; Vol. 1.
(12) Mitzi, D. B. In *Progress in Inorganic Chemistry*; Karlin, K. D., Ed.; John Wiley & Sons: New York, 1999; Vol. 48, pp 1−121.
(13) Mallouk, T. E.; Gavin, J. A. *Acc. Chem. Res.* **1998**, *31*, 209−217.
(14) Ban, T.; Ohwaki, T.; Ohya, Y.; Takahashi, Y. *Angew. Chem., Int. Ed.* **1999**, *38*, 3324−3326.
(15) D'Souza, S. M.; Alexander, C.; Carr, S. W.; Waller, A. M.; Whitcombe, M. J.; Vulfson, E. N. *Nature* **1999**, *398*, 312−316.
(16) Aizenberg, J.; Black, A. J.; Whitesides, G. M. *Nature* **1999**, *398*, 495−498.

10.1021/cm010285u CCC: $22.00
Published on Web 03/13/2002

Transition metal oxides are significant because they provide a broad range of chemical compositions and exhibit attractive physicochemical properties.[20] In particular, mixed-valent manganese oxides represent attractive substrates for assembly of nanoscale preparations. This is due to semiconducting[21] and magnetic properties[22] and is because this material finds ubiquitous applications in such areas as battery design[23] and oxidation catalysis.[24] This investigation is an extension of earlier communications reporting new advances in preparation and characterization of colloidal solutions of manganese oxide nanoparticles. The latter were observed as disks, ranging in size from 20 to 80 Å, with an average Mn oxidation state (AOS) of 3.70−3.79, and were generated via reduction of tetraalkylammonium permanganate salts in aqueous solution with 2-butanol.[25] These solutions undergo controlled gelation into well-characterized porous conducting helical wires, rings, and regular patterns.[26] For example, when placed in 3 mm i.d. capillaries, tetramethylammonium (TMA^+) permanganate salts in 2-butanol/H_2O sols form helical gels of composition $[N(CH_3)_4]^+_{0.93}Mn^{4+}_{2.1}Mn^{3+}_{1.9}O_7(OH)_{1.03}\cdot 5H_2O$ with a Mn AOS of 3.52 after heating at 85 °C for 160 h.[25] The amorphous sol starting material has been characterized by small angle neutron scattering to have homogeneous particle sizes on the order of 40−60 Å. The number of turns of these helices is primarily related to the starting concentration of the sol. The diameters of these helices can range from the millimeter range down to $<30\ \mu$m with lengths as long as 25 cm.[25] Examples of the helical morphology that have been produced by self-assembly of colloidal solutions of manganese oxide in capillary tubes of different diameters are shown in Figure 1.

At very low concentrations ($\sim 10^{-3}$ M), concentric ring patterns are formed on the walls of the capillary, and linear patterns on a flat glass surface.[25] Here we focus on AFM, EPR, and X-ray fluorescence quantitative studies of well-ordered linear patterns of manganese oxide deposited onto glass and quartz surfaces.

Experimental Section

Preparation of MnO_x Films on Flat Glass Surfaces. The H_2O/2-butanol colloidal solutions of lamellar MnO_x containing 0.1 M TMA and 0.025 M TEA permanganate were prepared according to published procedures.[25] These were diluted with distilled water to the desired concentrations of 2, 1, 0.75, and 0.5 mM in the Mn ion. For AFM studies the self-assembled lines of MnO_x were deposited on either 22 × 22 mm^2 glass microscope cover slips from Fisher or 25 × 25 mm^2 cover slips obtained from Corning Glass.

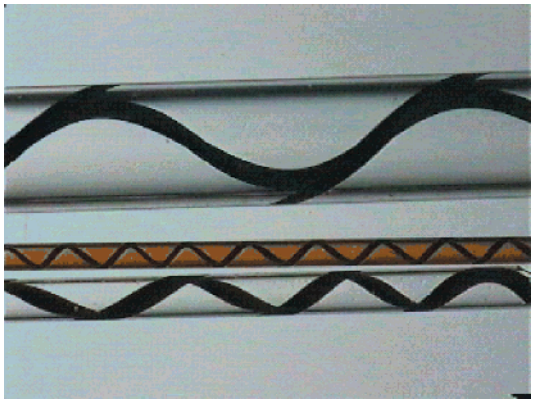

Figure 1. Helical morphologies produced by self-assembly of 0.1 M (in Mn) colloid in capillary tubes of 1.2, 0.5, and 0.2 mm i.d.

The cover slips were heated and fused to the bottom of T-shaped fused capillaries and adjusted to be strictly perpendicular to the bottom of a 30-mL beaker, without touching the bottom. Typically, the total length of the capillary with the attached cover slip was about 5.5 cm (3.3-cm capillary stem with a 22-mm cover slip attached) or 3.0 cm stem (with a 25-mm cover slip attached). It was found that on average about half of the glass plates placed in the colloid form smeared deposits of MnO_x film and no discernible linear patterns. Often that was the result of slides sticking together during the evaporation process, from adventitious dust particles in the solution prepared for evaporation and/or from occasional gross variations in evaporation rate due to fluctuations of house vacuum.

To prepare a sample, the T-shaped capillaries with an attached cover slip were placed (centered) into a 30-mL beaker, usually two at a time. To prevent the motion of the capillary/slip assembly, the rim of a beaker was coated with high-vacuum grease. The beaker was then placed into the preheated low-vacuum oven held at 79 ± 1 °C, and 20 mL of colloid was transferred into the beaker using a 10-mL pipet. The oven was evacuated using a house vacuum system, typically 12−20 psi below atmospheric pressure. Beakers were left undisturbed for 4−5 h to allow complete evaporation of water and drying of samples (at the rate of about 3−4 mL/h).

The center third of the cover slip was cut and mounted onto an AFM stub for analysis. All samples were examined the day they were prepared and stored in either air or a vacuum desiccator. It was observed that the texture of the sides of cover slips greatly influences the appearance of the lines. If the sides possess defects such as chips or irregular surfaces, the lines will not in general be straight.

Preparation of MnO_x Films on Quartz Surfaces. For EPR studies, the linear patterns of MnOx were deposited onto the outer surface of either a quartz EPR tube or quartz plates. For deposition onto the surface of tubes, the latter were attached with Teflon tape to a stirring rod resting on the lip of a tall 200-mL beaker (pregreased) such that the tube hung parallel to the sides of the beaker. Quartz plates (42 mm × 10 mm) were ordered from Wilmad Glass Co. The plates were ground to ~5 mm width, fire-polished, and glued into a slit of a small cork with LOC-TITE 495 glue. The cork was inserted into a glass tube and suspended in the colloid solution. The deposition was conducted as described above. The linear patterns deposited on the outer surface of the quartz tube were identical in optical appearance, thickness, and frequency to those found on the cover slips, deposited from the colloidal

(17) (a) Tremel, W. *Angew. Chem., Int. Ed. Engl.* **1999**, *38*, 2175−2179. (b) Kim, S. S.; Zhang, W.; Pinnavaia, T. J. *Science* **1998**, *282*, 1302−1305. (c) Huo, Q.; Zhao, F.; Weston, K.; Buratto, S. K.; Stucky, G. D.; Schacht, S.; Schuth, F. *Adv. Mater.* **1997**, *9*, 974−978.

(18) (a) Akiyama, Y.; Mizukami, F.; Kiyozumi, Y.; Maeda, K.; Izutsu, H.; Sakaguchi, K. *Angew. Chem., Int. Ed. Engl.* **1999**, *38*, 1420−1422. (b) Barsoum, M. W.; Farber, L. *Science* **1999**, *284*, 937−939.

(19) Engelkamp, H.; Middelbeek, S.; Nolte, R. J. M. *Science* **1999**, *284*, 785−788.

(20) Antonelli, D. M.; Trudeau, M. *Angew. Chem., Int. Ed. Engl.* **1999**, *38*, 1471−1474.

(21) Caneschi, A.; Gatteschi, D.; Sessoli, R. *J. Chem. Soc., Dalton Trans.* **1997**, 3963−3970.

(22) (a) Matthews, S.; Ramesh, R.; Venkatesan, T.; Benedetto, J. *Science* **1997**, *276*, 328−340. (b) Mahesh, R.; Mehendrian, R.; Raychaudhuri, A. K.; Rao, C. N. R. *J. Solid State Chem.* **1996**, *122*, 448−450. (c) Wolfman, J.; Simon, Ch.; Hervieu, M.; Maignan, A.; Raveau, B. *J. Solid State Chem.* **1996**, *123*, 413−416.

(23) Besenhard, J. O. In *Soft Chemistry Routes to New Materials-Chimie Douce*; Rouxel, J., Tournoux, M., Brec, R., Eds.; Trans. Tech: Aedermannsdorf, 1994; pp 152−153.

(24) Suib, S. L. In *Studies in Surface Science and Catalysis*; Chon, H., Woo, S. H., Park, S. E., Eds.; Elsevier: Amsterdam, 1996; Vol. 102, pp 47−74.

(25) Brock, S. L.; Sanabria, M.; Suib, S. L.; Urban, V.; Thijyagarajan, P.; Potter, D. *J. Phys. Chem. B* **1999**, *103*, 7416−7428.

(26) Giraldo, O.; Brock, S. L.; Marquez, M.; Suib, S. L.; Hillhouse, H.; Tsapatsis, M. *Nature* **2000**, *405*, 38−38.

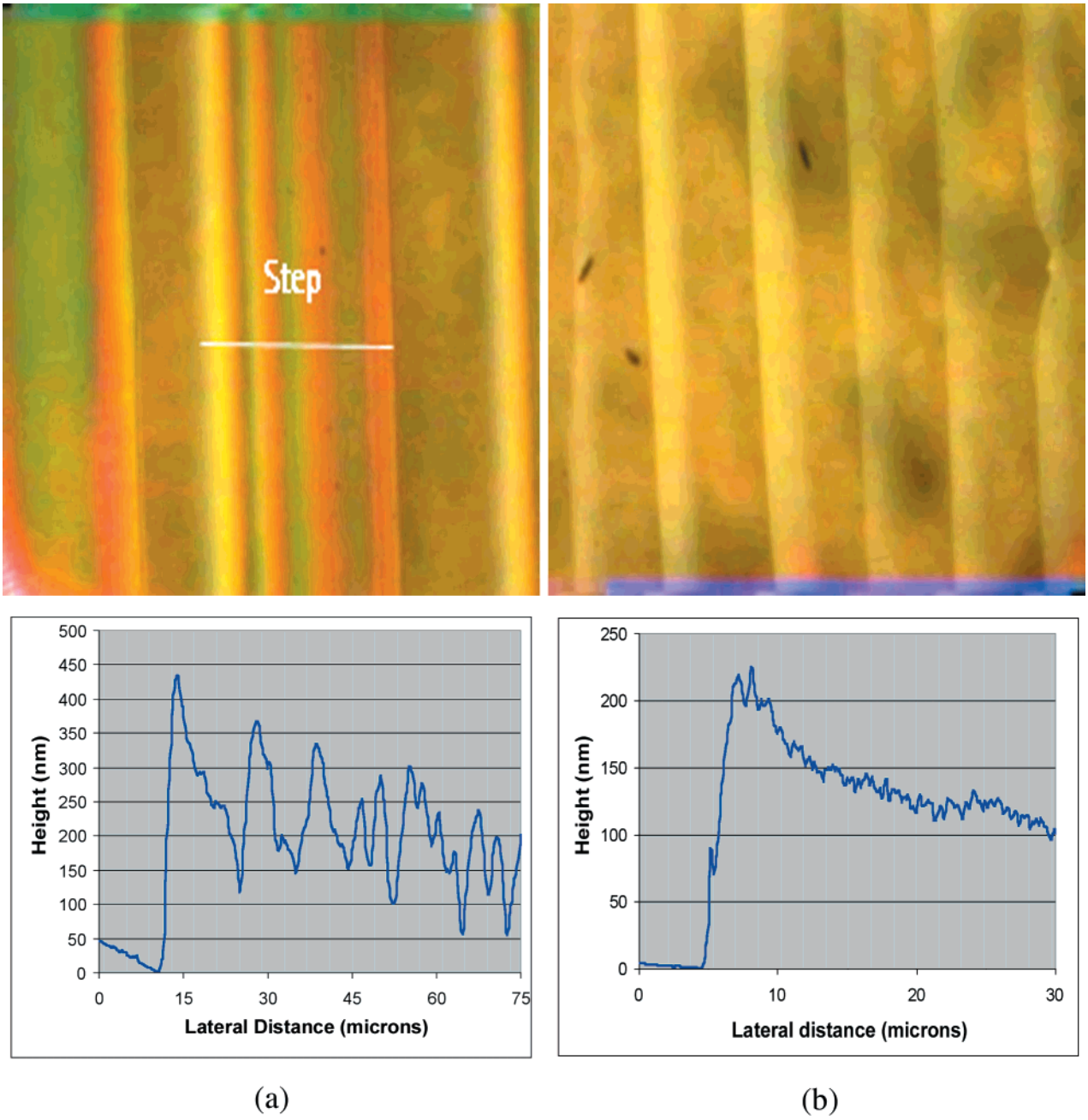

Figure 2. (a) Variation in surface topography for a line demonstrating color bands. The top of the figure is the optical image of lines on a cover slip; the bottom is the AFM image and cross-sectional profile graph. (b) Surface topography for a line that shows no color bands. The top of the figure is the optical image of lines on a cover slip; the bottom is the AFM image and cross-sectional profile graph.

solution of identical concentrations, under similar evaporation conditions.

Results

Several techniques were employed in order to determine the structural and chemical nature of the MnO_x films. AFM was used to study the morphology and the quantitative structure of the films, while EPR and X-ray techniques were employed to study the chemical nature of the material.

AFM−Optical Characterization of Samples. Using a Digital Instruments Nanoscope E atomic force microscope with an integrated CCD camera, optical images of the patterns were correlated with surface topography. Figure 2 illustrates this correlation. Figure 2a shows an optical image of a sample prepared from a 4×10^{-3} M concentration solution evaporated at 60°. A MnO_x line, approximately 180 μm in width, is seen on the image, which spans a 500 × 500 μm^2 area. The darker, more uniformly colored regions are the flat glass substrate. The parallel color bands observed on the line were found to be caused by optical interference effects due to differences in surface topography on the line. The cross-sectional perspective of the line measured by AFM justifies this conclusion. Surface topography variations which vary from 10 to 150 nm are observed to run parallel with the line and correlate with the color bands observed in the optical images. These color bands are observed for all samples produced using solutions with greater than 1×10^{-3} M. Figure 2b shows an optical

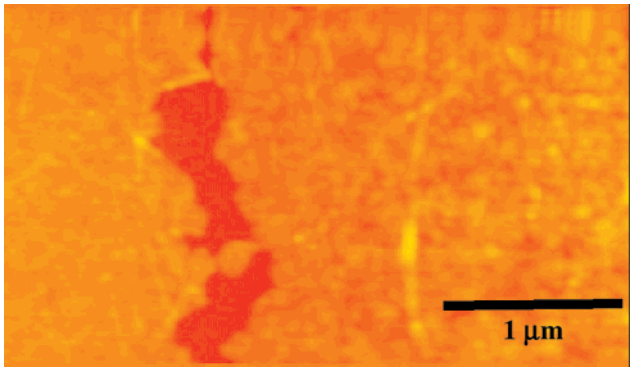

Figure 3. AFM image taken at the edge of a MnO_x line on a flat glass surface.

image of MnO_x lines formed from a 1×10^{-4} M concentration solution. No color bands are observed, and the AFM measurements show no surface topography variations on the line.

A closer examination of the patterned material with AFM illustrates the structure of the lines. Figure 3 shows a 4 μm AFM image of the edge of a line. The dark region in the center of the image is a crack in the film revealing the flat glass substrate. The line can be seen to be composed of small agglomerations of material, approximately 100 nm in size. These agglomerations are also seen to combine into chains of material.

X-ray Fluorescence. On the basis of the dimensions of ordinary X-ray beams, chemical analysis of the lines found in our samples would not be possible because of very small line cross sections. Although the total volume of the line is large, the sampling volume is determined by the cross section of only 70 μm. However, by employing a X-ray microbeam from an undulator on the MHATT-CAT Sector at the Advanced Photon Source, a large number of X-ray photons were focused down to a submicron cross-sectional area while maintaining beam brilliance.[27] The undulator X-ray beam was focused to 1 μm^2 for these measurements. Mechanical manipulators allowed the sample to be translated in orthogonal directions in a plane containing the axis of the line. Through systematic translations of the sample in the $x-y$ plane and with respect to the beam, a full X-ray fluorescence pattern was recorded over a 160.0 μm $\times$ 240.0 μm area. The mapping took 4 h using a map grid resolution of 1-μm steps in x and y. The X-ray fluorescence data can then be analyzed for specific elements. Figure 4 shows a top view of these data. The area map shown in the figure represents the Mn fluorescence. The variation in Mn content can readily be seen over the area of the scan. This figure clearly shows that the line is not uniform with respect to chemical composition. Contour plots show the highest fluorescence signal off center of the line, by approximately 10% to the left. Examination of different areas of the line and other similar lines results in similar characteristic X-ray fluorescence patterns. These data establish the presence of Mn and the location of the Mn within the plane parallel to the line axis.

There also appears to be a slight inhomogeneity in the concentration of Mn along the line. Optical observations of lines reveal the presence of a thin, transparent layer of organic material on the leading and trailing edges of lines. This band of material is clearly visible on the trailing edge, a white stripe running along the length of the lines (see Figure 2). While it was desirable to locate the region of highest Mn concentration by X-ray fluorescence, the beam alignment procedure did not allow us to ascertain if the X-ray beam was scanned along the saw-tooth direction or in an opposite fashion. However, since the line appears to form a saw-tooth type topography (see AFM section above), it can be reasonably expected that the regions of maximum line thickness contain the highest concentration of Mn. Thus, the combination of the AFM, optical, and X-ray fluorescence studies does allow some correlation of the chemical composition of lines with their topography and morphology.

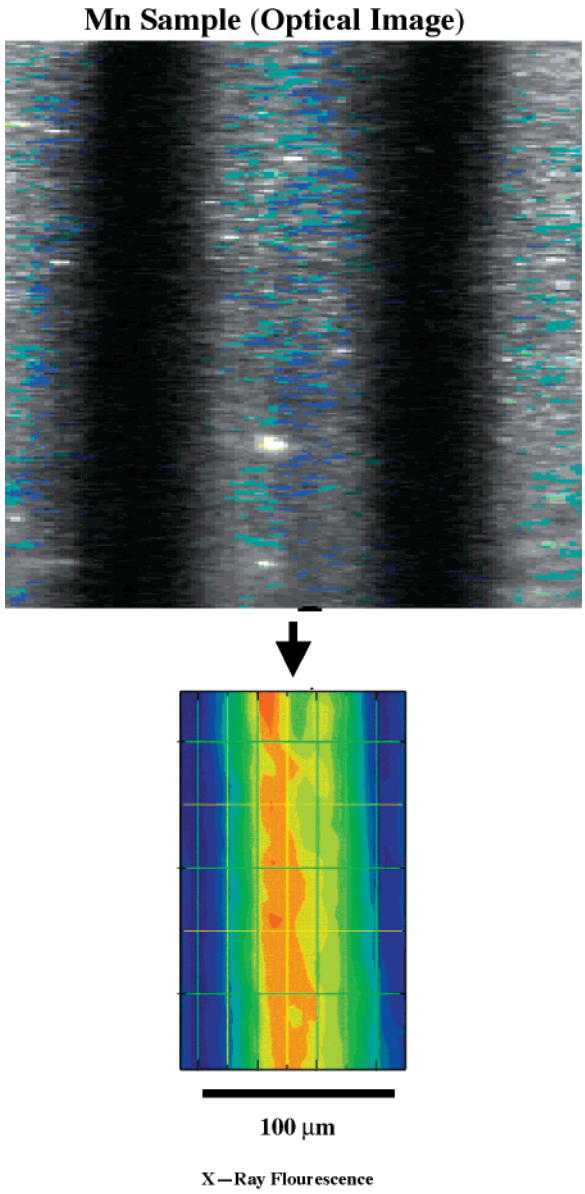

Figure 4. X-ray fluorescence map showing the concentration of Mn in the self-assembled MnO_x lines on a glass cover slip.

It must be noted that similar transparent organic material appears to also cover the entire surface of helical wires derived from these colloidal solutions. We are currently trying to prepare sufficient quantities of

(27) Ice, G. E.; Chung, J.-S.; Lowe, W.; Williams, E.; Edelman, J. *Rev. Sci. Instrum.*, in press.

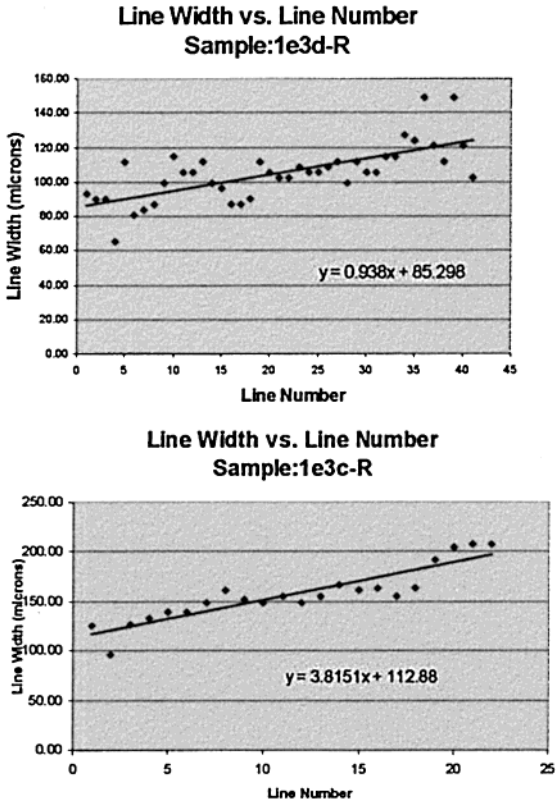

Figure 5. Comparison of the line width increases of two samples generated from a 1×10^{-3} M colloid solution.

this material for chemical characterization. This proved to be a surprisingly difficult task, since the gross amount of this material is small and it is very difficult to separate it from the helical wires or surface deposits.

Line Width Analysis and Molar Concentration Effects. A study of the variation in line width as a function of line number and concentration was performed using a Sony CCD optical video camera. Five locations on each line were randomly selected, and an average line width was calculated in order to average out irregularities in individual line widths. An individual line was found to vary from position to position by no more than 10%. Samples prepared from solution evaporated at 80° were used for all line width experiments described here.

For the sake of analysis, the top of the cover slip was designated as that part of the cover slip that did not have lines. The lines on the sample were numbered beginning with the first line from the top of the sample and increasing downward. Measurements of average line width versus line number show an increase in width as the sample line numbers increased. Figure 5 is a measurement of the line widths for a molar concentration of 1×10^{-3} M. All lines exhibited the trend seen in Figure 5 with the relative rate of the increase of width varied from sample to sample. This increase in line width with increasing line number is believed to be a consequence of the colloidal nature of the MnO_x solution. As the solvent evaporates, the concentration of the mixture increases, allowing for more particulate matter to adhere to the glass surface, making the lines wider as the process continues.

Systematic studies were also performed to investigate the variation in line width, frequency (in number of lines per centimeter), and height of the lines with varying concentration. Because of the variability in line width versus line number, only lines 3−7 on samples with concentrations varying from 1×10^{-4} to 4×10^{-3} M were compared. From data in Table 1, the line width is seen to consistently increase with increasing concentration of the sample. Data in Table 1 also show a significant correlation between the molar concentration and the average line frequency. The decrease in concentration clearly causes a significant increase in line frequency.

Table 1. Concentration Dependence of the Width, Frequency, and Height of the Self-Assembled MnO_x Line

concentration[a] ($\times 10^4$ M)	line width (μm)	line frequency (lines/cm)	line height (nm)
1.0		92 ± 10	
5.0	70 ± 2[b]		
7.6	110 ± 2		
10	150 ± 2	43 ± 5	276 ± 10
20	180 ± 2	43 ± 11	148 ± 10
40		29 ± 6	352 ± 10

[a] Concentration of Mn in the sol−gel solution. [b] All errors are listed as two standard deviations, calculated from at least 15 lines in at least 5 different samples deposited from solution at the concentration shown.

Time-Dependent Changes. The effects of sample storage and aging were studied for samples stored in air and in a vacuum desiccator. Samples prepared from 1×10^{-3} and 2×10^{-3} M concentration solutions were cut in half, with half stored in air and the other half stored in a vacuum desiccator. The image of the desiccated sample shows optical rings in the line that are believed to be formed from a liquid that was drawn out of the lines by the vacuum desiccator. The composition of the liquid is not known but supports the conclusion that these self-assembling lines form in a layered structure.[24] These aging and desiccation effects were found to be similar for various concentrations, scan locations, and environmental factors (such as humidity).

Finally, the line height measurements were observed to vary in a nonsystematic way with molar concentration. Measurements of height were complicated by its time-dependent nature. While the line width and frequency were observed to remain constant over time, the sample height and line mechanical properties changed with time. The line heights were observed to decrease significantly over the span of 1 week, and the lines were found to become much softer. After approximately 1 week, the AFM tip would deform the line surface, making measurements of the height difficult.

EPR Studies. Concentric lines of this material deposited on a quartz tube from 1×10^{-3} M colloids initially generated a weak, moderately wide room-temperature EPR signal (ca. 500 G); see Figure 6. Within 1 month, this signal increases by about 10-fold, and after 3 more months, the signal, while not increasing in intensity, sharpens to about 250 G perhaps because of exchange narrowing, as more organic radicals are generated at the surface.

Similar results are observed when the lines are deposited onto the surface of a flat quartz plate. Initially, no signal is observed. After approximately 2 months (Figure 7) the spectra showed a signal, also at $g = 2$, with the line width (250 G) similar to that observed from lines on a tube surface. The signal is

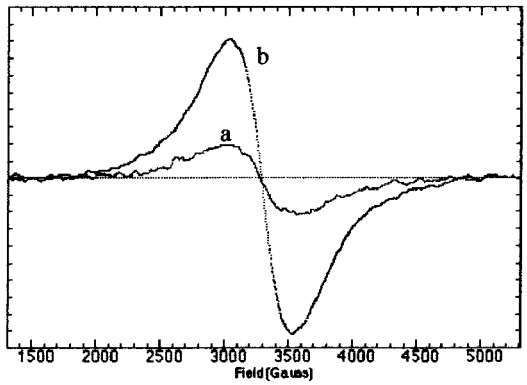

Figure 6. Room-temperature X-band EPR spectra of MnO_x lines deposited onto a 5 mm o.d. quartz EPR tube. The larger signal was obtained from the same sample after 33 days. Microwave frequency, 9.57 MHz; modulation amplitude, 10 G; power, 5 mW.

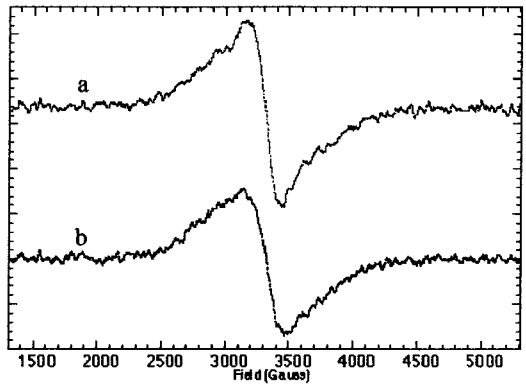

Figure 7. Room-temperature X-band EPR spectra of MnO_x lines deposited onto a quartz plate. The spectra were recorded after ca. 2 months as described in the text. Microwave frequency, 9.57 MHz; modulation amplitude, 10 G; power, 5 mW.

anisotropic, since the spectrum recorded with the field perpendicular to the plate surface (upper trace in Figure 7) is narrower than the one observed when the field is parallel to the surface. This indicates that there is some preferential alignment of organic radicals on the surface of MnO_x.

Discussion

There are two main aspects to the data discussed here. The data present a rather complex qualitative picture of the self-assembled lines deposited onto the cover slips. Nonetheless, the qualitative measurements suggest several important features of these deposits, consistent with their optical appearance. The quantitative aspect of the measurements can also be used to verify the existing theoretical models for the formation of these lines, currently under development by Chang et al.[28]

Even though the mixed-valent (III, IV) manganese oxide compounds are EPR-silent[29] unless measured in matrixes near 4 K,[30] the samples of helical wires obtained from gelation of concentrated colloids do exhibit a very wide (in excess of 2000 G) room-temperature signal at $g = 2$ without any detectable hyperfine splitting. Our samples likely exhibit a similar, weaker signal. Such spectra are difficult to interpret and most likely arise from an overlap of Mn^{2+} signals and those of radicals resulting from slow oxidation of organic material (2-butanol, 2-butanone, and trialkylamines) by (III, IV) manganese oxides. Nonetheless, the AFM and EPR measurements are highly consistent with the proposed layered structure of the lines.[24] The lines are found to decrease in height upon aging, suggesting the peeling of the outer layers of lamellar MnO_x particles (ca. 100 nm structures observed by AFM). We further observe (on aging in a desiccator) an emission of a liquid trapped between the layers. It is highly likely that the material trapped between the layers is organic, since the EPR shows an increasing signal from this material as the sample is aged. This is almost certainly due to the slow oxidation of the trapped organic molecules such as the unreacted isobutanol and product 2-butanone. It is likely that this process occurs at the surface of lamellar manganese oxide layers, resulting in a dense local concentration of radicals whose signal is broadened by dipolar magnetic interactions.[31] This organic material may also be a part of the transparent outer coating of the lines (see X-ray Fluorescence section above). However, no chemical characterization of the coating was possible because of the very small amount (a few nanometer-sized droplets) available. The EPR data indicate that the organic radicals trapped between the layers of the MnO_x are partially oriented. Thus, it may be possible to utilize these self-assembled lines as a template for ordered magnetic materials.

Our X-ray fluorescence and quantitative AFM data are also consistent with a physical model currently being developed by Chang. Briefly, a wetting colloidal fluid generates a thin film protruding beyond the contact line. Self-assembled line formation occurs first near the contact line, since the film is thinner and the concentration of MnO_x is higher. The forming line consumes most of the ions in the film, and diffusion is insufficient to resupply material from the bulk of the liquid below. As a result, line formation stops after a finite stripe is formed at the contact (liquid) line. The contact line recedes as the evaporation continues, leaving behind a stripe. The film thins as it recedes, eventually reaching the saturation concentration required to start the deposition of the next stripe. Qualitatively, X-ray and AFM data support this picture, since the lines are asymmetric, both in their height and Mn concentration. Quantitatively, the increase in line width with increasing concentration is also consistent with this model. As the concentration of the solution increases, there is faster replacement (by diffusion) of the precipitating material at the edge of the liquid line until it is completely exhausted, and a break appears between the lines. This would cause an increase in line width, as is observed experimentally (Table 1). Similarly, an increase in line width is expected as the solution evaporates, because of the increase in colloid concentration. Again, this is observed experimentally, as the line width

(28) Chang, H. C. University of Notre Dame, Physics Department, private communication.

(29) De Guzman, R. N.; Shen, Y.-F.; Shaw, B. R.; Suib, S. L.; O'Young, C.-L. *Chem. Mater.* **1993**, *5* (10), 1395−1400.

(30) Ferrante, R. F.; Wilkerson, J. L.; Graham, W. R.; Weltner, W. *J. Chem. Phys.* **1977**, *67* (12), 5904−5913.

(31) Abragam, A.; Bleaney, B. *Electron Paramagnetic Resonance of Transition Ions*; Dover: New York, 1986; pp 529−535.

of the self-assembled lines roughly doubles as the line number increases 10-fold (see Figure 5). However, this model would predict that the line frequency would increase with increasing concentration, since the thinning out of the receding liquid film would generate a saturated solution faster, thus hastening the formation of the next line. As can be seen from Table 1, this appears not to be the case, as the line frequency definitely decreases with increasing concentration of the sol−gel. At the present time, we think that this is a consequence of line width increase; that is, the diminishing line frequency is balanced by the fact that the lines are much wider, perhaps necessitating longer times for the evaporation and saturation of the receding film (severely depleted of the solute), thus delaying the onset of the next line.

The mechanism discussed here is somewhat similar to the phenomena observed by Lu et al. in the course of particle formation from the soluble silica/surfactant systems. They have observed the formation of mesostructured nanoparticles from both the thin films[32] and aerosol droplets.[33] In both cases, the nanoparticles are formed by selective evaporation of the alcohol, resulting in silica−surfactant micelle formation and coassembly of the latter into liquid-crystalline mesophases. This is quite complex and requires not only a concentration gradient but also the maintenance of the liquid or liquid-crystalline state during the course of evaporation. Formation of the linear patterns described here and in ref 25 appears to proceed by a simpler process, although it is quite possible that in our case selective evaporation of the 2-butanol also takes place. The model discussed above does not require this to happen, since the formation of the MnO_x lines results from simple superconcentration of the solution. The complexity of the method utilized by Lu et al. enables precise control resulting in generation of silica-based vesicular, cubic, and hexagonal mesostructures. The system described here is useful for generating ordered liner patterns and spiral microwires of Mn-based material, thus extending the variety of nanoassemblies available from sol−gel preparations.

CM010285U

(32) Lu, Y.; Fan, H.; Stump, A.; Ward, T. L.; Reiker, T.; Brinker, C. J. *Nature* **1997**, *389*, 364−368.

(33) Lu, Y.; Fan, H.; Stump, A.; Ward, T. L.; Reiker, T.; Brinker, C. J. *Nature* **1999**, *398*, 223−226.